

Renormalized Mutual Information for Artificial Scientific Discovery

Leopoldo Sarra,^{1,2,*} Andrea Aiello,¹ and Florian Marquardt^{1,2}

¹Max Planck Institute for the Science of Light, Erlangen, Germany

²Department of Physics, Friedrich-Alexander Universität Erlangen-Nürnberg, Germany

(Dated: November 8, 2021)

We derive a well-defined renormalized version of mutual information that allows to estimate the dependence between continuous random variables in the important case when one is deterministically dependent on the other. This is the situation relevant for feature extraction, where the goal is to produce a low-dimensional effective description of a high-dimensional system. Our approach enables the discovery of collective variables in physical systems, thus adding to the toolbox of artificial scientific discovery, while also aiding the analysis of information flow in artificial neural networks.

Introduction. – One of the most useful general concepts in the analysis of physical systems is the notion of collective coordinates. In many cases, ranging from statistical physics to hydrodynamics, the description of a complex many-particle system can be dramatically simplified by considering only a few collective variables like the center of mass, an order parameter, a flow field, or vortex positions. However, in new situations, it is not clear a priori which low-dimensional “feature” $y = f(x)$ is best suited as a compact description of the high-dimensional data x . This is the domain of unsupervised feature extraction in computer science, where large datasets like images or time series are to be analyzed [1]. Future frameworks of artificial scientific discovery [2–5] will have to rely on general approaches like this, adding to the rapidly developing toolbox of machine learning for physics [6–8].

The simplest and most known algorithm to obtain such features is the Principal Component Analysis (PCA) [9]. The idea is to project the input into the directions of largest variance. However, its power is limited, since it can only extract linear features. A general approach to estimate the quality of a proposed feature is given by Mutual Information [10, 11]. In general, the mutual information $I(x, y)$ answers the following question: if two random variables y and x are dependent on one another, and we are provided with the value of y , how much do we learn about x ? Technically, it is defined via $I(x, y) = I(y, x) = H(y) - H(y|x)$, where $H(y|x)$ is the conditional entropy of y given x [11]. Maximization of mutual information can be used to extract “optimal” features [12], as sketched in Fig. 1.

There exists, however, a well-known important problem in evaluating the mutual information for *continuous* variables with a *deterministic* dependence [13, 14], which is exactly the case relevant for feature extraction. In this case, $I(x, y)$ diverges, and it is not clear how to properly cure this divergence without losing important properties of I . Specifically, reparametrization invariance turns out to be crucial: applying a bijective function to obtain $y' = g(y)$ does not change the information content, and thus $I(x, y') = I(x, y)$.

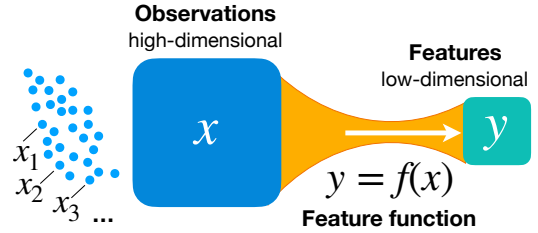


Figure 1. Feature extraction, where a high-dimensional “microscopic” description x (such as the configuration of a many-particle system) is mapped to a low-dimensional feature $y = f(x)$. This is the case where the renormalized mutual information presented in this article is needed for feature optimization.

In this work, we introduce a properly *renormalized* version of mutual information for the important case of feature extraction with continuous variables:

$$\tilde{I}(x, y) = H(y) - \int dx P_x(x) \ln \sqrt{\det \nabla f(x) \cdot \nabla f(x)} \quad (1)$$

where $x \in \mathbb{R}^N$, $y = f(x) \in \mathbb{R}^K$; we use $\nabla f(x) \cdot \nabla f(x)$ as a short-hand notation for $(\sum_i \partial_i f_\mu \partial_i f_\nu)_{\mu\nu}$, with $1 \leq i \leq N$ and $1 \leq \mu, \nu \leq K$, i.e. the $K \times K$ matrix resulting from the product of the $(K \times N)$ Jacobian matrix $\nabla f(x)$ and its transpose. The quantity \tilde{I} is well-defined and finite. In addition, it preserves fundamental properties of mutual information – among which the invariance under reparametrization of the features:

$$\tilde{I}(x, g(y)) = \tilde{I}(x, y), \quad (2)$$

for a bijective function $g : \mathbb{R}^K \rightarrow \mathbb{R}^K$. We will derive and discuss below the meaning and usefulness of the renormalized quantity \tilde{I} .

Mutual information is used in many cutting edge machine learning applications, helping to improve the intermediate layers of a neural network [15, 16], to increase the interpretability of Generative Adversarial Networks [17], to analyze the behavior of neural networks during training [18, 19] through the Information Bottleneck method [20, 21], and for feature extraction via mutual information optimization [22]. It can be also used to characterize

* leopoldo.sarra@mpl.mpg.de

the variables in a renormalization group procedure [23]. Its practical estimation is not trivial [24], but recently derived bounds [25] permit its evaluation even in high-dimensional spaces, with the help of neural networks [26].

However, there is a problem with deterministically-dependent continuous features: the conditional entropy $H(y|x)$ formally diverges as $-\log \delta(0)$ whenever y is a deterministic function of x . To understand why, it is enough to take its definition, $H(y|x) = -\int dx dy P_x(x) P(y|x) \ln P(y|x)$, and plug in $P(y|x) = \delta(y - f(x))$. This is specific to continuous variables: with discrete variables, conditional entropy would be zero and mutual information would coincide with the entropy of one of the variables. It is clear that, to deal with a deterministic continuous dependence, it is necessary to somehow redefine mutual information. Past remedies involved adding noise to the feature y or (equivalently) to simply consider the non-diverging term $H(y)$ [22, 27], as briefly suggested in the InfoMax seminal paper [12]. However, they all lead to a very undesirable property: they break the fundamental reparametrization invariance of mutual information. In this scheme, any two features can be made to have the same entropy $H(y)$ simply by rescaling. Thus, in the context of feature optimization, they would be considered equally favorable, even if they represent very different information about x . The reason is that such a scheme completely ignores the diverging quantity $H(y|x)$. In contrast, we show that $H(y|x)$ contains a non-trivial finite dependence on the feature $f(x)$, which must be taken into account to obtain consistent results.

Renormalized Mutual Information. – In any physical system, there are small pre-existing measurement uncertainties associated with extracting the microscopic observables x . Thus, loosely speaking, when trying to deduce information about x given the value of y , we have to be content with resolving x up to some spread ε . Motivated by this, we first consider a finite regularized quantity $I_\varepsilon(x, y)$. It is defined as the mutual information between the observable x and the feature function applied to a noisy version of the observable: $y = f(x + \varepsilon\lambda)$, where $\varepsilon \in \mathbb{R}$ is the noise strength and $\lambda \in \mathbb{R}^N$ is a random multidimensional Gaussian of zero mean and unit covariance matrix. In the limit $\varepsilon \rightarrow 0$ we recover the original definition of mutual information, which diverges logarithmically. Even in that limit, the nature of the adopted noise distribution (e.g. isotropy, independence of x) still matters, and corresponds to imposing some hypotheses about the observed quantities x (e.g. same measurement uncertainty in all variables). We discuss these generalizations at the end of this work.

Consider

$$P(y|x) = \int d\lambda P_\lambda(\lambda) \delta(y - f(x + \varepsilon\lambda)). \quad (3)$$

When $\varepsilon \ll 1$, we can expand $f(x + \varepsilon\lambda) \simeq f(x) + \varepsilon\lambda \cdot \nabla f(x)$. By explicit calculation, it can be easily found that $P(y|x)$ is a Gaussian distribution of zero mean and covariance

matrix $\varepsilon^2 \nabla f(x) \cdot \nabla f(x) = \varepsilon^2 (\sum_i \partial_i f_\mu \partial_i f_\nu)_{\mu\nu}$. We can calculate the conditional entropy and get

$$H(y|x) = \int dx P_x(x) \ln \sqrt{\det \nabla f(x) \cdot \nabla f(x)} + KH_\varepsilon, \quad (4)$$

where H_ε is the entropy of a one-dimensional Gaussian with variance ε^2 . The first term only depends on the features, and the second only on the noise. Only this term diverges when $\varepsilon \rightarrow 0$. Therefore

$$\tilde{I}_\varepsilon(x, y) = I_\varepsilon(x, y) + KH_\varepsilon \quad (5)$$

has a well defined limit $\varepsilon \rightarrow 0$ and still contains all the dependence on $f(x)$. By performing the limit we obtain our main result, Eq. (1).

We can easily show that Eq. (1) is invariant under feature reparametrization. Consider an invertible function $z = g(y) : \mathbb{R}^K \rightarrow \mathbb{R}^K$. We can rewrite the entropy of z as the entropy of y plus an extra term, which cancels with that obtained by differentiating $\ln \det(\nabla g(f(x)))$, leading to Eq. (2). We emphasize the importance of this property: after an invertible transformation on the variable y , no information should be lost, and the new variable should have the same mutual information with x as the old one. In contrast, by adding Gaussian noise η to the feature y instead of to x , i.e. $y = f(x) + \varepsilon\eta$, the final result would depend on the feature only via $H(y)$. Reparametrization invariance would not hold anymore under this alternative regularization: we have $I_\varepsilon(x, g(f(x) + \varepsilon\eta)) = I_\varepsilon(x, f(x) + \varepsilon\eta)$ but not $I_\varepsilon(x, g(f(x)) + \varepsilon\eta) = I_\varepsilon(x, f(x) + \varepsilon\eta)$ as Eq. (2) would require.

The price for a finite mutual information between two deterministically-dependent variables is that when there is no dependence, e.g. $y = \text{const.}$, we get $-\infty$ instead of 0. In addition, given the different roles that x and y play, renormalized mutual information is no longer symmetric in its arguments. From a different perspective [28], Eq. (1) can be expressed as a particular kind of *Information Loss* [29, 30].

Mutual information obeys inequalities like $I(x, (y_1, y_2)) \geq I(x, y_1)$, which translate to the regularized version I_ε . However, naively taking $\varepsilon \rightarrow 0$ results in an empty inequality $\tilde{I}(x, (y_1, y_2)) + \infty \geq \tilde{I}(x, y_1)$. By contrast, starting from $I(x, (y_1, y_2)) \geq I(x, y_1) + I(x, y_2) - I(y_1, y_2)$, we can take the same limit and obtain a useful finite result:

$$\tilde{I}(x, (y_1, y_2)) \geq \tilde{I}(x, y_1) + \tilde{I}(x, y_2) - I(y_1, y_2). \quad (6)$$

In the special case where the dimensions of y_1 and y_2 add up to the dimension of x , and the mapping $x \mapsto (y_1, y_2)$ is bijective, reparametrization invariance produces $\tilde{I}(x, (y_1, y_2)) = \tilde{I}(x, x) = H(x)$, and so

$$H(x) \geq \tilde{I}(x, y_1) + \tilde{I}(x, y_2) - I(y_1, y_2). \quad (7)$$

If one constructs y_2 to be independent of y_1 , the third term on the right-hand side vanishes. However, it would

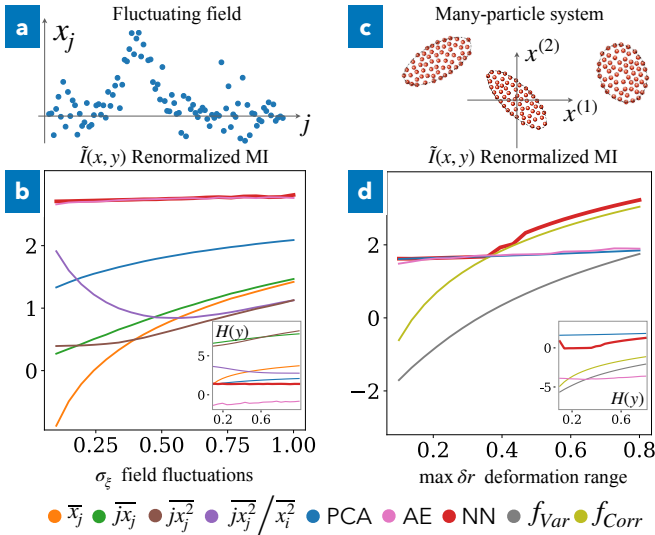


Figure 2. Comparing renormalized mutual information \tilde{I} for several features in two representative physical scenarios. (a) Fluctuating 1D field on a lattice, with a randomly placed “wave packet” (we depict one single sample). (b) \tilde{I} as a function of the size of the field fluctuations σ_ϵ for several features. Let $\bar{A}_j = \frac{1}{N} \sum_{j=1}^N A_j$. We consider: the average field $f(x) = \bar{x}_j$, the position j weighted by the field amplitude, $\overline{jx_j}$, or weighted by the field intensity, $\overline{jx_j^2}$, as well as the “normalized” feature $\overline{jx_j^2/x_j^2}$ (similar to an expectation value in quantum mechanics) and the first PCA component. (c) Two-dimensional “drops” with elliptical shapes of fixed area but with fluctuating deformation amplitude δr and orientation θ (we depict three samples). (d) \tilde{I} vs. max. deformation spread for the 2d-feature given by PCA and for two nonlinear features sensitive to shape deformations, $f_{Var} = \overline{((x_j^{(1)})^2, (x_j^{(2)})^2)}$ and $f_{Corr} = \overline{((x_j^{(1)})^2, x_j^{(1)}x_j^{(2)})}$, where $x_j^{(1)}, x_j^{(2)}$ are the coordinates of particle j . In both (b) and (d): AE represents the bottleneck of a contractive autoencoder trained to reconstruct the input and NN corresponds to the feature given by a neural network optimized to maximize \tilde{I} . In the insets, we show the entropy $H(f(x))$. This quantity is not reparametrization invariant.

be impermissible to drop $\tilde{I}(x, y_2)$, since it can have any sign.

Feature comparison. – The renormalized mutual information can be used to find out how useful any given “macroscopic” quantity (i.e. a feature $y = f(x)$) would be in characterizing the system. The result depends on the statistical distribution of x . It might be the Boltzmann distribution in equilibrium or a distribution of “snapshots” of the system configuration during some arbitrary time evolution. When control parameters such as temperature or external fields change the distribution of x , the optimal feature can change. Intuitively, observing a feature with higher \tilde{I} is more effective in narrowing down the set of underlying configurations x compatible with the observed value, thus yielding more information about the system.

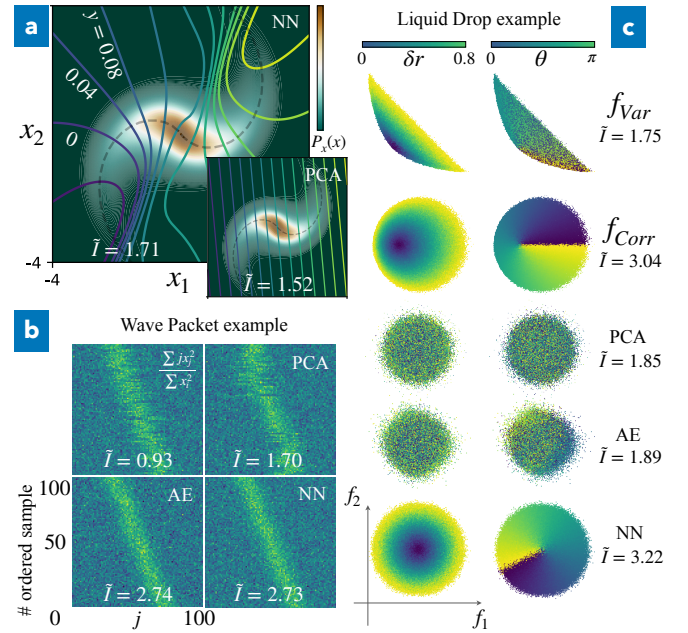


Figure 3. Feature optimization and visual assessment of quality. (a) 2D non-Gaussian distribution. The obtained 1D feature $y = f(x_1, x_2)$, shown as contour lines atop the distribution $P_x(x)$, is parametrized with a neural network. Inset: PCA feature. (b) Wave packets as in Fig. 2a, one by row, ordered by increasing value of the feature. The NN feature is clearly very powerful to sort the samples. (c) Liquid drops as in Fig. 2c. We show how different 2D features map the deformation and the orientation of the drop. The NN builds up a representation very similar to our best handcrafted feature f_{Corr} .

We show proof-of-concept examples in the most common domains of physics that deal with many degrees of freedom: fluctuating fields and many-particle systems. One important goal is to discover, without prior knowledge, that a given fluctuating field is dominated by certain localized excitations (like solitons and vortices) and to robustly estimate their properties (position, shape, velocity, etc.). The simplest example is a 1D field on a lattice with a wave packet of fixed shape at a random position (Fig. 2a,b) [31]. For now, we evaluate \tilde{I} for a variety of handcrafted features, turning to feature optimization further below. Because of reparametrization invariance (Eq. (2)), the scaling of any of them is irrelevant, as is any bijective nonlinear transformation. For comparison, we also consider PCA [9], which in our context corresponds to a feature $f(x) = \sum_j x_j u_j$, where u is the eigenvector associated to the largest eigenvalue of the covariance matrix $\langle x_i x_j \rangle - \langle x_i \rangle \langle x_j \rangle$, and the bottleneck of a contractive autoencoder [32].

In a many-particle system (molecule, star cluster, plasma, etc.), the goal is to discover the most meaningful collective coordinates. A simple prototypical example is a liquid drop of fluctuating shape and orientation, made of atoms with known force fields (Fig. 2c,d).

Feature optimization. – Instead of comparing different

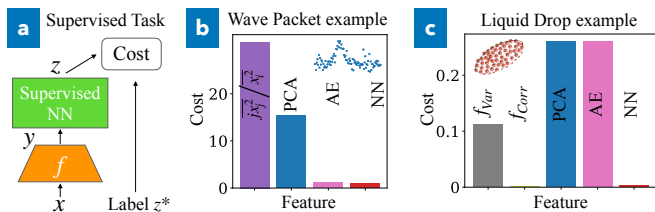


Figure 4. Comparing the performance of a supervised regression task for different features as input. (a) For each batch of samples x we calculate the feature $y = f(x)$ and train a supervised neural network to predict the provided label z^* . (b) Predicting the center of the wave packet (example from Fig. 2a). (c) Predicting the orientation and deformation of the drop (example from Fig. 2c). The optimized NN feature achieves the best performance in (b) and a performance very close to that of our best handcrafted feature (c).

plausible features, we can consider a class of parametrized features and optimize \tilde{I} over the parameters. We opted for a multilayer neural network [33], where $f(x) = f_\theta(x)$ with θ representing the parameters of the network. Intuitively, meaningful features are those that provide the largest information without over-engineering. While handcrafted features, like in the previous section, are unarguably simple, the optimization of an excessively powerful feature function could lead to encode additional (non-relevant) information by means of very non-linear transformations. The tradeoff between the simplicity of the feature and the amount of preserved information can be adjusted both by the choice of network architecture and by adding a small additional regularization penalty (in practice, this can be achieved by punishing features with large gradients). The optimization of $\tilde{I}(x, f_\theta(x))$ can be implemented easily with gradient ascent algorithms [33]. The first term in Eq. (1) can be estimated with a histogram; for the second term, one can immediately obtain the required ∇f , since neural networks are differentiable functions, and rely on statistical sampling of x . Note that also the extra degree of freedom of feature space due to reparametrization invariance (Eq. 2) can be exploited to enforce additional constraints [34].

In Fig. 3a we show the optimization of a nonlinear 1D feature for a 2D non-Gaussian distribution. Such a low-dimensional setting allows to visualize the shape of the feature and to compare it with PCA. We apply the same technique also to the physical examples (see "NN" in Fig. 2b, d).

One way to assess the quality of features is by suitable visualization (see Fig. 3b, c). The optimized NN feature is clearly able, better than (or at least as good as) other features, to identify the relevant properties of the system. A more quantitative, well-known approach is to perform supervised training for a regression task with the feature as input and analyze the resulting performance [35]. In the physics examples shown here, one is naturally interested in predicting underlying parameters, like the wave packet location. Fig. 4b, c illustrate superior or very

good performance of the network.

In our illustrative examples we only considered 1D or to 2D features. For higher-dimensional features, the numerical estimation of Eq. (1) is more challenging, but in principle still feasible [36], for example through adversarial techniques [37].

Also, all the components x_j had the same physical meaning (e.g. particle coordinates). For components with different dimensions (e.g. positions and momenta), one needs to decide how to compare fluctuations along different components. A slight change in the regularization procedure is required. Most generally, we can consider the noise distribution $P(\lambda|x)$ to have an arbitrary covariance matrix $\Sigma(x)$, even allowing for a location-dependent "resolution". We find that it is necessary to replace the matrix $\nabla f(x) \cdot \nabla f(x)$ in Eq. (1) with $\nabla f(x)\Sigma(x)\nabla f(x)$, thus effectively introducing a metric on x -space [38]. This changes the inequality mentioned above (Eq. (7)).

Outlook. – Renormalized mutual information can be useful in many areas of statistical analysis, machine learning, and physics.

It can be directly applied in diverse physical scenarios, with many interesting variations and extensions. In statistical physics, one expects that different phases of matter yield different optimal features. Moreover, one could optimize for feature *fields* (order parameter fields) by using convolutional layers in the neural network. The locations of defects like domain walls and vortices could be discovered as relevant features. In general, an optimized low-dimensional description of a high-dimensional system can be used to make partial predictions for the time evolution. In dynamical systems the renormalized mutual information could help to discover the underlying regularities of the system. Even in the presence of chaos, the evolution of collective variables can be predictable (and still non-trivial) [39]. Quantum-mechanical systems could be analyzed as well, e.g. by sampling configurations x according to a many-body state, or sampling parameters in the Hamiltonian and looking at the expectation values x of a set of commuting observables in the corresponding ground state.

Renormalized mutual information can be used to analyze deterministic representations of a dataset. Here we illustrated the approach only in settings with at most two-dimensional features, but it should be feasible to efficiently evaluate \tilde{I} also with high-dimensional feature spaces. This approach could be used to study the behavior of a neural network from an information-theoretic perspective, for example by analyzing the renormalized mutual information between the input and an intermediate layer of a neural network. This could be helpful for concepts like the "information bottleneck" [20, 40], which is known to be affected by the problems we discussed. Moreover, the important challenge of representation learning for high-dimensional datasets (like images) can benefit: our optimized features are purely defined by their information content and not by the capability to

accomplish selected tasks. Thus, they could be useful in transfer learning scenarios, in which many classifiers are built from the same representation. We emphasize that the method advocated here should be especially useful when the dimensionality is so drastically reduced that autoencoders [32, 41, 42] would not plausibly work very well, since it would be impossible for a decoder to pro-

duce an approximation of the input from so few latent variables (see Fig. 3c). This is precisely the situation important for collective variables and similar strongly reduced descriptions.

The code of this paper is publicly available [43].

Acknowledgements. – We thank Andreas Maier for discussions.

-
- [1] Y. Bengio, A. Courville, and P. Vincent, Representation Learning: A Review and New Perspectives, *IEEE Trans. Pattern Anal. Mach. Intell.* **35**, 1798 (2013).
- [2] R. D. King, J. Rowland, S. G. Oliver, M. Young, W. Aubrey, E. Byrne, M. Liakata, M. Markham, P. Pir, L. N. Soldatova, A. Sparkes, K. E. Whelan, and A. Clare, The Automation of Science, *Science* **324**, 85 (2009).
- [3] M. Schmidt and H. Lipson, Distilling Free-Form Natural Laws from Experimental Data, *Science* **324**, 81 (2009).
- [4] T. Wu and M. Tegmark, Toward an artificial intelligence physicist for unsupervised learning, *Phys. Rev. E* **100**, 033311 (2019).
- [5] R. Iten, T. Metger, H. Wilming, L. del Rio, and R. Renner, Discovering Physical Concepts with Neural Networks, *Phys. Rev. Lett.* **124**, 010508 (2020).
- [6] V. Dunjko and H. J. Briegel, Machine learning and artificial intelligence in the quantum domain, arXiv:1709.02779 [quant-ph] (2017).
- [7] P. Mehta, M. Bukov, C.-H. Wang, A. G. Day, C. Richardson, C. K. Fisher, and D. J. Schwab, A high-bias, low-variance introduction to Machine Learning for physicists, *Phys. Rep.* **810**, 1 (2019).
- [8] G. Carleo, I. Cirac, K. Cranmer, L. Daudet, M. Schuld, N. Tishby, L. Vogt-Maranto, and L. Zdeborová, Machine learning and the physical sciences, *Rev. Mod. Phys.* **91** (2019).
- [9] I. T. Jolliffe and J. Cadima, Principal component analysis: a review and recent developments, *Philosophical Transactions of the Royal Society A: Mathematical, Physical and Engineering Sciences* **374**, 20150202 (2016).
- [10] T. Cover and J. A. Thomas, *Elements of information theory*, 2nd ed. (Wiley-Interscience, Hoboken, N.J., 2006).
- [11] A. Papoulis and S. U. Pillai, *Probability, random variables, and stochastic processes*, 4th ed. (McGraw-Hill, Boston, Mass., 2009).
- [12] A. J. Bell and T. J. Sejnowski, An Information-Maximization Approach to Blind Separation and Blind Deconvolution, *Neural Comput.* **7**, 1129 (1995).
- [13] R. A. Amjad and B. C. Geiger, Learning Representations for Neural Network-Based Classification Using the Information Bottleneck Principle, *IEEE Trans. Pattern Anal. Mach. Intell.* , 1 (2019).
- [14] A. Kolchinsky, B. D. Tracey, and S. V. Kuyk, Caveats for information bottleneck in deterministic scenarios, in *International Conference on Learning Representations* (2019).
- [15] R. D. Hjelm, A. Fedorov, S. Lavoie-Marchildon, K. Grewal, P. Bachman, A. Trischler, and Y. Bengio, Learning deep representations by mutual information estimation and maximization, arXiv:1808.06670 [cs, stat] (2018).
- [16] M. Tschannen, J. Djolonga, P. K. Rubenstein, S. Gelly, and M. Lucic, On Mutual Information Maximization for Representation Learning, in *International Conference on Learning Representations* (2020).
- [17] X. Chen, Y. Duan, R. Houthoofd, J. Schulman, I. Sutskever, and P. Abbeel, InfoGAN: Interpretable Representation Learning by Information Maximizing Generative Adversarial Nets, in *Proceedings of the 30th International Conference on Neural Information Processing Systems, NIPS16* (Curran Associates Inc., Red Hook, NY, USA, 2016) pp. 2180–2188.
- [18] R. Shwartz-Ziv and N. Tishby, Opening the Black Box of Deep Neural Networks via Information, arXiv:1703.00810 [cs] (2017).
- [19] A. M. Saxe, Y. Bansal, J. Dapello, M. Advani, A. Kolchinsky, B. D. Tracey, and D. D. Cox, On the information bottleneck theory of deep learning, *J. Stat. Mech: Theory Exp.* **2019**, 124020 (2019).
- [20] N. Tishby, F. C. Pereira, and W. Bialek, The information bottleneck method, in *Proc. of the 37-th Annual Allerton Conference on Communication, Control and Computing* (1999) pp. 368–377.
- [21] M. Gabrié, A. Manoel, C. Luneau, J. Barbier, N. Macris, F. Krzakala, and L. Zdeborová, Entropy and mutual information in models of deep neural networks, *J. Stat. Mech: Theory Exp.* **2019**, 124014 (2019).
- [22] S. S. Haykin, *Neural networks: a comprehensive foundation*, 2nd ed. (Prentice Hall, Upper Saddle River, N.J., 1999).
- [23] M. Koch-Janusz and Z. Ringel, Mutual information, neural networks and the renormalization group, *Nat. Phys.* **14**, 578 (2018).
- [24] A. Kraskov, H. Stögbauer, and P. Grassberger, Estimating mutual information, *Phys. Rev. E* **69**, 066138 (2004).
- [25] B. Poole, S. Ozair, A. Van Den Oord, A. Alemi, and G. Tucker, On Variational Bounds of Mutual Information, in *Proceedings of the 36th International Conference on Machine Learning*, Proceedings of Machine Learning Research, Vol. 97, edited by K. Chaudhuri and R. Salakhutdinov (PMLR, Long Beach, California, USA, 2019) pp. 5171–5180.
- [26] M. I. Belghazi, A. Baratin, S. Rajeshwar, S. Ozair, Y. Bengio, A. Courville, and D. Hjelm, Mutual Information Neural Estimation, in *Proceedings of the 35th International Conference on Machine Learning*, Proceedings of Machine Learning Research, Vol. 80, edited by J. Dy and A. Krause (PMLR, Stockholm, Sweden, 2018) pp. 531–540.
- [27] G. Deco and D. Obradovic, *An Information-Theoretic Approach to Neural Computing*, edited by J. Taylor and C. Mannion, Perspectives in Neural Computing (Springer New York, New York, NY, 1996).
- [28] See Supplemental Material at [URL will be inserted by publisher] for the equation of Renormalized Mutual In-

formation in terms of information loss.

- [29] B. C. Geiger and G. Kubin, On the Information Loss in Memoryless Systems: The Multivariate Case, in *Proc. Int. Zurich Seminar on Communications* (2011) pp. 32–35.
- [30] B. C. Geiger, C. Feldbauer, and G. Kubin, Information loss in static nonlinearities, in *2011 8th International Symposium on Wireless Communication Systems* (IEEE, Aachen, Germany, 2011) pp. 799–803.
- [31] See Supplemental Material at [URL will be inserted by publisher] for technical details on the examples.
- [32] S. Rifai, P. Vincent, X. Muller, X. Glorot, and Y. Bengio, Contractive Auto-Encoders: Explicit Invariance during Feature Extraction, in *Proceedings of the 28th International Conference on International Conference on Machine Learning*, ICML’11 (Omnipress, Madison, WI, USA, 2011) pp. 833–840.
- [33] I. Goodfellow, Y. Bengio, and A. Courville, *Deep Learning* (MIT Press, 2016).
- [34] See Supplemental Material at [URL will be inserted by publisher] for technical details on the numerical implementation of neural-network-based feature optimization.
- [35] See Supplemental Material at [URL will be inserted by publisher] for the technical details of the implementation.
- [36] See Supplemental Material at [URL will be inserted by publisher], section V for more details.
- [37] I. Goodfellow, J. Pouget-Abadie, M. Mirza, B. Xu, D. Warde-Farley, S. Ozair, A. Courville, and Y. Bengio, in *Advances in Neural Information Processing Systems 27*, edited by Z. Ghahramani, M. Welling, C. Cortes, N. Lawrence, and K. Weinberger (Curran Associates, Inc., 2014) pp. 2672–2680.
- [38] See Supplemental Material at [URL will be inserted by publisher] for the derivation of the general case with position-dependent noise.
- [39] D. Forster, *Hydrodynamic Fluctuations, Broken Symmetry, and Correlation Functions*, 1st ed. (CRC Press, 2018).
- [40] D. Strouse and D. J. Schwab, The Deterministic Information Bottleneck, *Neural Comput.* **29**, 1611 (2017).
- [41] G. Hinton, Reducing the Dimensionality of Data with Neural Networks, *Science* **313**, 504 (2006).
- [42] P. Vincent, H. Larochelle, Y. Bengio, and P.-A. Manzagol, Extracting and Composing Robust Features with Denoising Autoencoders, in *Proceedings of the 25th International Conference on Machine Learning*, ICML ’08 (Association for Computing Machinery, New York, NY, USA, 2008) pp. 1096–1103.
- [43] <https://github.com/lisarra/rmi>.
- [44] Martín Abadi, et al., Paul Barham, Eugene Brevdo, Zhifeng Chen, Craig Citro, Greg S. Corrado, Andy Davis, Jeffrey Dean, Matthieu Devin, Sanjay Ghemawat, Ian Goodfellow, Andrew Harp, Geoffrey Irving, Michael Isard, Y. Jia, Rafal Jozefowicz, Lukasz Kaiser, Manjunath Kudlur, Josh Levenberg, Dandelion Mané, Rajat Monga, Sherry Moore, Derek Murray, Chris Olah, Mike Schuster, Jonathon Shlens, Benoit Steiner, Ilya Sutskever, Kunal Talwar, Paul Tucker, Vincent Vanhoucke, Vijay Vasudevan, Fernanda Viégas, Oriol Vinyals, Pete Warden, Martin Wattenberg, Martin Wicke, Yuan Yu, and Xiaoqiang Zheng, *TensorFlow: Large-Scale Machine Learning on Heterogeneous Systems* (2015).
- [45] T. Hastie, R. Tibshirani, and J. Friedman, *The elements of statistical learning: data mining, inference, and prediction: with 200 full-color illustrations*, Springer series in statistics (Springer, New York, 2001).
- [46] D. P. Kingma and J. Ba, Adam: A Method for Stochastic Optimization, in *3rd International Conference on Learning Representations, ICLR 2015, San Diego, CA, USA, May 7-9, 2015, Conference Track Proceedings*, edited by Y. Bengio and Y. LeCun (2015).

Appendix A: Derivation of Renormalized Mutual Information for the general case of position-dependent noise

In this section, we derive the renormalized mutual information equation,

$$\tilde{I}(x, y) = H(y) - \int dx P_x(x) \ln \sqrt{\det(\nabla f(x) \cdot \nabla f(x))}, \quad (\text{A1})$$

in the general case in which the regularizing noise also depends on x . We consider the observable distribution $x \sim P_x(x)$, with $x \in \mathbb{R}^N$. Let λ be the noise variable. It has a zero-mean Gaussian distribution with covariance matrix $\Sigma(x)$. If we have no assumptions on the observables, we can just choose $\Sigma(x) = \mathbb{I}_N$. Let $\varepsilon \in \mathbb{R}$ represent the strength of the noise. At the end of the calculation, we perform the limit $\varepsilon \rightarrow 0$. First of all, we define the feature

$$y = f(x + \varepsilon\lambda).$$

Its probability distribution is given by

$$P_y(y) = \int dx P_x(x) d\lambda P_\lambda(\lambda|x) \delta(y - f(x + \varepsilon\lambda)).$$

By definition, $P_\lambda(\lambda|x)$ is a Gaussian distribution with zero mean. The contribution of large values of λ in the δ -function are suppressed by the factor $P_\lambda(\lambda|x)$. As a consequence, when $\varepsilon \approx 0$, we can consider the expansion of the feature function, $f(x + \varepsilon\lambda) \approx f(x) + \varepsilon \nabla f(x) \cdot \lambda$. We employ the Fourier representation of the δ -function

$$\delta(y) = \frac{1}{(2\pi)^k} \int ds e^{isy}$$

and plug in the expression of the distribution of the noise,

$$P(\lambda|x) = \frac{1}{\sqrt{(2\pi)^N \det(\Sigma(x))}} e^{-\frac{1}{2}\lambda\Sigma(x)^{-1}\lambda}.$$

We get

$$P(y|x) = \int \frac{ds}{(2\pi)^k} e^{is(y-f(x))} \int \frac{d\lambda}{\sqrt{(2\pi)^N \det(\Sigma(x))}} e^{-\frac{1}{2}\lambda\Sigma(x)^{-1}\lambda - is\varepsilon\nabla f(x)\cdot\lambda} = \int \frac{ds}{(2\pi)^k} e^{-\frac{\varepsilon^2}{2}s(\nabla f(x)\Sigma(x)\nabla f(x))s + i(y-f(x))s}.$$

Now, we can also perform the Gaussian integral in s and get

$$P(y|x) = \frac{1}{\sqrt{(2\pi\varepsilon)^k \det(\nabla f(x)\Sigma(x)\nabla f(x))}} e^{-\frac{1}{2\varepsilon^2}(y-f(x))(\nabla f(x)\Sigma(x)\nabla f(x))^{-1}(y-f(x))}.$$

This is a Gaussian distribution with mean $f(x)$ and covariance matrix $\varepsilon\nabla f(x)\Sigma(x)\nabla f(x)$. By explicit calculation, the conditional entropy $H(y|x)$ is given by

$$H(y|x) = - \int dx dy P_x(x) P_y(y|x) \ln P(y|x) = \frac{K}{2} \ln 2\pi\varepsilon\varepsilon^2 + \frac{1}{2} \int dx P_x(x) \ln \det(\nabla f(x)\Sigma(x)\nabla f(x)).$$

We define

$$\tilde{I}(x, y) = \lim_{\varepsilon \rightarrow 0} [H(y) - H(y|x) + KH_\varepsilon] = H(y) - \int dx P_x(x) \ln \sqrt{\det(\nabla f(x)\Sigma(x)\nabla f(x))},$$

with $H_\varepsilon = \frac{1}{2} \ln 2\pi\varepsilon\varepsilon^2$. This equation is more general than Eq. (A1) and reduces to it if we consider an isotropic noise matrix, i.e. $\Sigma(x) = \mathbb{I}_N$.

Appendix B: Reparametrization Invariance

In this section, we verify that renormalized mutual information is invariant under feature reparametrization. Consider an invertible function $g(y) : \mathbb{R}^K \rightarrow \mathbb{R}^K$ and the associated random variable $z = g(y)$. Renormalized mutual information between x and z can be expressed as

$$\tilde{I}(x, z) = H(z) - \int dx P_x(x) \ln \sqrt{\det(\nabla g(f(x)) \cdot \nabla g(f(x)))}. \quad (\text{B1})$$

By employing the properties of differential entropy, we can rewrite

$$H(z) = H(y) + \int dx P_x(x) \ln \det \left(\frac{dg}{dy} \right).$$

The second term of Eq. (B1) can be expanded via the chain rule of differentiation

$$\nabla g(f(x)) = \frac{dg}{dy} \cdot \nabla f(x)$$

and by using the properties of the determinant

$$\det(\nabla g(f(x)) \cdot \nabla g(f(x))) = \left(\det \frac{dg}{dy} \right)^2 \det(\nabla f(x) \cdot \nabla f(x)).$$

By putting all together, we get

$$\tilde{I}(x, z) = H(y) - \int dx P_x(x) \ln \sqrt{\det(\nabla f(x) \cdot \nabla f(x))} = \tilde{I}(x, y)$$

as we wanted to show.

Appendix C: Connection with Information Loss

The concept of *information loss* was introduced in a series of interesting papers [29, 30], as the difference between two mutual informations, $I(x, y) - I(x, z)$, where the random variables y and z are functions of the random variable x . The key point is that both $I(x, y)$ and $I(x, z)$ formally diverge, but their difference remains finite. Here we show that our renormalized mutual information can be interpreted as an information loss.

Indeed, the diverging mutual information $I(x, y = f(x))$ can be made finite in at least two different ways: either by adding noise to the input variables to obtain $I(x, y = f(x + \varepsilon\lambda_x))$, or by adding noise to the output variables to get $I(x, z = f(x) + \varepsilon\lambda_y)$. Here we assume that both λ_x and λ_y are Gaussian variables with zero mean and unit variance (with proper dimension). A straightforward calculation shows that in the limit $\varepsilon \ll 1$ we have

$$I(x, f(x + \varepsilon\lambda_x)) = H(y) - KH_\varepsilon - \int dx P_x(x) \ln \sqrt{\det(\nabla f(x) \cdot \nabla f(x))}, \quad (\text{C1})$$

$$I(x, f(x) + \varepsilon\lambda_y) = H(y) - KH_\varepsilon, \quad (\text{C2})$$

with $H_\varepsilon = \frac{1}{2} \ln 2\pi e\varepsilon^2$.

By subtracting the second equation from the first one and adding $H(y)$, we see that the divergent term KH_ε cancels out, and that we obtain a relation between our *finite* renormalized mutual information and the information loss:

$$\tilde{I}(x, f(x)) = H(y) + \lim_{\varepsilon \rightarrow 0} [I(x, f(x + \varepsilon\lambda_x)) - I(x, f(x) + \varepsilon\lambda_y)]. \quad (\text{C3})$$

According to [29, 30] the limit above represents the information lost by changing the description of x from $f(x + \varepsilon\lambda_x)$ to $f(x) + \varepsilon\lambda_y$.

Appendix D: Examples

In this section, we give some technical details about the examples shown in the main text. The two specific examples that we described are illustrative of two of the most important domains of physics that deal with many degrees of freedom: fluctuating fields and many-particle systems. They are conceptually as simple as possible, requiring no specialized prior knowledge.

1. Spiral-shaped distribution

The example in Fig. 3a of the main text has no particular physics background. It is just a simple example in which unconstrained feature optimization can be visualized directly. We consider a two-dimensional Gaussian distribution (with zero mean) and perform the transformation

$$\begin{cases} x_1 = x'_1 \cos \alpha r' - x'_2 \\ x_2 = x'_1 \sin \alpha r' + x'_2 \end{cases}$$

where $r' = \sqrt{(x'_1)^2 + (x'_2)^2}$, and α is a fixed parameter. In our implementation, the covariance matrix of the initial Gaussian is

$$\begin{pmatrix} 0.64 & -0.56 \\ -0.56 & 1 \end{pmatrix}$$

and $\alpha = 0.5$.

2. Wave Packet

The example in Fig. 2a consists in the superposition of a fluctuating field and a packet with a fixed shape. In particular, each sample is given by

$$x_j = \xi_j + e^{-(j-\bar{j})^2/\delta j^2}, \quad j = 1, \dots, N \quad (\text{D1})$$

with ξ_j i.i.d. Gaussian random variables, $\delta j = 9$, \bar{j} uniformly random $\in [30, 70]$, $N = 100$.

3. Liquid Drop

The example in Fig.2c is built by first choosing a uniform random deformation $\delta r \in [0, 0.8]$ and orientation $\theta \in [0, \pi]$. An ellipse with axis $A = R + \delta R$ and $B = \frac{R^2}{R + \delta R}$ and rotated by an angle θ is considered. The axes are chosen so that the area of the ellipse is fixed to πR^2 for any δr . N particles are placed randomly inside the ellipse. Subsequently, we turn on a Lennard-Jones interaction between the particles

$$V(\|\mathbf{d}_{ij}\|) = \begin{cases} -\frac{\|\mathbf{d}_{ij}\|^2}{d_{\text{coll}}^2} + \frac{3}{2} + \frac{1}{2} \left(\frac{d_{\text{eq}}}{d_{\text{coll}}}\right)^{2n} - \left(\frac{d_{\text{eq}}}{d_{\text{coll}}}\right)^n & \|\mathbf{d}_{ij}\| < d_{\text{coll}} \\ \frac{1}{2} \left(\frac{d_{\text{eq}}}{\|\mathbf{d}_{ij}\|}\right)^{2n} - \frac{1}{2} \left(\frac{d_{\text{eq}}}{\|\mathbf{d}_{ij}\|}\right)^n + \frac{1}{2} & \|\mathbf{d}_{ij}\| \geq d_{\text{coll}} \end{cases}$$

where \mathbf{d}_{ij} is the distance between two particles, d_{coll} is a cutoff at small distances and d_{eq} represents the equilibrium distance between two particles. We also add a boundary potential that constrains the particles inside the drop

$$V(\mathbf{r}_i) = \begin{cases} W\|\mathbf{r}_i\| & \text{outside the ellipse} \\ 0 & \text{inside the ellipse} \end{cases}$$

where $\mathbf{r}_i = (x_i^{(1)}, x_i^{(2)})$ is the coordinate of a particle. We simulate the relaxation of the system by performing some gradient descent steps; a stochastic term is added to emulate a finite temperature T : we update the position of each particle as

$$\mathbf{r}'_i = \mathbf{r}_i + \eta \nabla_i V + \sqrt{2\eta T} \xi_i,$$

where ξ_i is a random Gaussian variable (zero mean, unit variance) and η represents the step size of the thermalization. In particular, we chose $R = 1$, $N = 60$, $n = 6$, $d_{\text{eq}} = 0.27$, $d_{\text{coll}} = 0.06$, $W = 200$, $\eta = 10^{-5}$. We performed $2 \cdot 10^3$ thermalization steps.

Appendix E: Feature Extraction in a Low-Dimensional Setting

Here, we show how we implemented the optimization of Eq. (A1) to extract the features in the *Feature optimization* section of the main text. In particular, we extract a one- or two-dimensional feature. In a low-dimensional feature setting, it is feasible to discretize the feature space y in a lattice, with lattice constant Δy in the 1d case or $\Delta y_1, \Delta y_2$ in the 2d case. We keep $f(x)$ continuous and we parametrize it with a neural network, i.e. $f(x) = f_\theta(x)$, where θ are the weights and the biases of the neurons of the network. In particular, we quickly recall that a neural network is made of many concatenated layers, and that each layer involves the application of a non-linear function σ (called activation function) to a linear combination of the inputs: we can write the output of a layer of input \mathbf{x} (and parameters $\theta = (\mathbf{w}, b)$) as

$$\sigma(\mathbf{w} \cdot \mathbf{x} + b).$$

To implement Eq. (A1) in TensorFlow [44], we need to write it as a differentiable function. By looking at Eq. (A1), we see that the first term $H(y)$ must be approximated in some way; the second term can be directly used.

The easiest way to approximate $H(y)$ is to first estimate $P_y(y)$, and then use it to compute the sum $H(y) = -\Delta y \sum_k P_y(y_k) \log P_y(y_k)$ (where $\Delta y = \Delta y_1 \Delta y_2$ in the 2d feature case). We approximate the probability density $P_y(y)$ with a Kernel Density Estimation procedure [45]: we apply a kernel $K_j(y)$ on each point $y_j = f(x_j)$ and write

$$P_y(y) = \frac{1}{N} \sum_j K_j(y),$$

where N is the number of points in the batch. Now we can discretize $P_y(y)$ by assigning to each element of the lattice y_k

$$P_y(y_k) = \int_{y_k - \frac{\Delta y}{2}}^{y_k + \frac{\Delta y}{2}} dy P_y(y), \quad k = 1, \dots, k_f. \quad (\text{E1})$$

In other words, instead of assigning each point to a single bin of the histogram, this function assigns it to all the bins, in a way proportional to the kernel applied to the point. In this way, we can always calculate analytically the result of

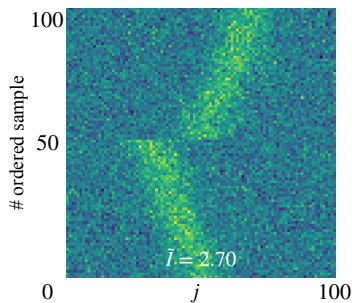


Figure 5. Non-smooth feature in the case of the example in section D2. We show wave packets as in Fig. 2a of the main text, one by row, ordered by increasing value of the feature. Without the regularizing term in Eq. E2 the optimization can get stuck in local minima that have almost the same \tilde{I} as the optimal feature (compare with Fig. 3b of the main text). As a consequence, the network can assign different feature values to very similar samples, while still being able to distinguish them.

the integral in Eq. (E1) as the difference of two Error functions. In practice, we use a Gaussian kernel with variance $(s\Delta y)^2$, i.e.

$$K_j(y) = \frac{1}{\sqrt{(2\pi s^2 \Delta y^2)^d}} e^{-\left(\frac{y - f(x_j)}{s\Delta y}\right)^2}$$

(where d is the dimension of y) and we empirically chose $s = 1$ in the 1D case and $s = 2$ in the 2D case. In the 1D case we discretize the feature in $k_f = 180$ bins, in the 2D example we use $k_f = 100$. We fix the bounds of the histogram so that it always includes all the points.

The optimization of Eq. (A1) is performed through gradient descent in the following way. We define the cost function that we want to minimize, $C = -\tilde{I}(x, f_\theta(x))$. At each step, we consider a batch of samples, calculate $f_\theta(x)$ for all the points in the batch and use it to estimate $P_y(y)$. We calculate $\tilde{I}(x, y = f_\theta(x))$ and use backpropagation to update each parameter of the neural network, i.e. an update rule

$$\theta_{n+1} = \theta_n - \eta \frac{\partial C}{\partial \theta},$$

where n is the training step and the learning rate η is a fixed parameter of the algorithm, trying to converge to the minimum of the cost function. In practice, one can obtain better performance by using more advanced algorithms like RMSprop or Adam [46].

We can improve the smoothness of the extracted feature by adding to the cost function an exponentially decaying term that penalizes large gradients:

$$Ae^{-\frac{\eta}{\tau} \langle \|\nabla f_\theta(x)\| \rangle_x} \quad (\text{E2})$$

where $\langle a(x) \rangle_x = \int dx P_x(x) a(x)$, and A and τ are hyperparameters that should be chosen conveniently. This can prevent extracting features that almost have the optimal information content but present discontinuities (see for example Fig. 5).

In addition, we remind that because of reparametrization invariance (Eq. (B1)) we can arbitrarily choose the density distribution of the output feature. For example, we can enforce a Gaussian feature distribution (with zero mean and variance σ^2) by adding to the cost function the Kullback-Leibler divergence [33] of a Gaussian with the feature distribution:

$$B(KL(P_y||\mathcal{G})) = B\left(\int dy P_y(y) \log \frac{P_y(y)}{\mathcal{G}(y)}\right) = B\left(-H(y) - \frac{1}{2\sigma^2} \langle y^2 \rangle_{y \sim P_y(y)}\right). \quad (\text{E3})$$

where B is a hyperparameter that can be chosen freely. This increases the accuracy of the feature entropy because it prevents the output distribution to condense in very small regions, making our estimate unreliable. To sum up, the cost function that we minimize, including all possible regularizations that we described, reads as

$$C = -\tilde{I}(x, f_\theta(x)) + Ae^{-\frac{\eta}{\tau} \langle \|\nabla f_\theta(x)\| \rangle_x} + B(KL(P_y||\mathcal{G})). \quad (\text{E4})$$

Table I shows the parameters we used in the examples described in Fig. 3 of the main text.

Spiral-shaped distribution			Wave packet			Liquid drop		
Layer	Neurons	Activation	Layer	Neurons	Activation	Layer	Neurons	Activation
input	2	-	input	100	-	input	120	-
layer 1	30	tanh	layer 1	70	tanh	layer 1	800	relu
layer 2	30	tanh	layer 2	70	tanh	output	2	linear
output	1	linear	output	1	linear			
cost	\tilde{I}		cost	\tilde{I}		cost	\tilde{I}	
optimizer	Adam		optimizer	Adam		optimizer	RMSprop	
learning rate	$5 \cdot 10^{-3}$		learning rate	$5 \cdot 10^{-3}$		learning rate	$5 \cdot 10^{-3}$	
batch size	100		batch size	700		batch size	$5 \cdot 10^3$	
training steps	$3 \cdot 10^4$		training steps	$1.5 \cdot 10^4$		training steps	$3 \cdot 10^4$	
regularization: A	0	(see Eq. E2)	regularization: A	10^2	(see Eq. E2)	regularization: A	15	(see Eq. E2)
regularization: B	5	(see Eq. E3)	regularization: τ	10^3	(see Eq. E2)	regularization: τ	500	(see Eq. E2)
			regularization: B	5	(see Eq. E3)	regularization: B	$5 \cdot 10^{-2}$	(see Eq. E3)

Table I. Layout and training parameters of the network used for feature optimization. (left) Spiral-shaped distribution as in Section D 1. (middle) Wave packet as in Section D 2. (right) Liquid drop as in Section D 3. When we used the gradient regularization as in Eq. E2, we always carried the optimization until the term completely decayed and was irrelevant in the final part of the training.

Improving feature extraction

In this paper, we optimized renormalized mutual information to extract only a one- or two-dimensional feature. As shown in the previous section, we could use a histogram-like approximation of the entropy term in Eq. (A1). Generalizations to high-dimensional feature settings will clearly require to find a better way to estimate $H(y)$. One more advanced option to estimate it is to exploit adversarial techniques. One could introduce a reference distribution $P_r(y)$ and rewrite $H(y) = -\langle \ln P_r(y) \rangle_{y \sim P_y(y)} - KL(P_y || P_r)$, where the last term is the Kullback-Leibler divergence [33] between $P_r(y)$ and $P_y(y)$. This term can be estimated by means of adversarial techniques [37], i.e. by optimizing over an auxiliary “discriminator” neural network $D(y)$:

$$H(y) = -\langle \ln P_r(y) \rangle_{y \sim P_y(y)} + \min_D \left(\langle D(y) \rangle_{y \sim P_y(y)} + \langle e^{-D(y)} \rangle_{y \sim P_r(y)} - 1 \right).$$

For convenience, $P_r(y)$ can be chosen as a Gaussian distribution. This is related to the technique proposed in [26] to estimate mutual information, while properly allowing for the renormalization discussed here.

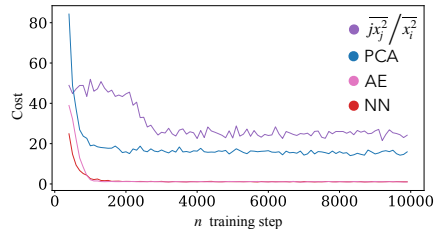
Appendix F: Autoencoders

Autoencoders [33] are a particular state-of-the-art kind of neural network intended for representation learning in unsupervised settings. They have two parts: an Encoder, which takes the input x and outputs a lower dimensional representation $f(x)$, the feature, also called latent space or bottleneck, and the Decoder, which takes the latent representation $f(x)$ and whose output has the same dimension of the input. This neural network is optimized so that the output matches the input. Since the bottleneck has a lower dimension than the input and output, only an insightful representation will allow to optimally reconstruct the input. We used a particular kind of autoencoder called Contractive Autoencoder [32], which should encourage more robust features. Apart from minimizing the mean squared error between the input and the reconstructed output, it also includes a term that penalises the Frobenius norm of the Jacobian of the bottleneck:

$$\lambda \|\nabla f(x)\|^2.$$

In our experiments, we consider the feature provided by the output of the encoder (i.e. the function that maps the input to the bottleneck), after the autoencoder has been trained. We used the same networks described in Table I for

Supervised Network - Wave Packet		
Layer	Neurons	Activation
input	1	-
layer 1	50	relu
layer 2	50	relu
output	1	linear
<hr/>		
cost	MSE	
optimizer	Adam	
learning rate	10^{-3}	
batch size	200	
training steps	10^4	



Feature	\tilde{I}	Cost
f_E	0.93	31.0
PCA	1.71	15.4
AE	2.75	1.12
NN	2.73	1.05

Figure 6. Performance comparison of the supervised task in Fig. 4b of the main text. (left) Structure of the supervised neural network and optimization parameters. (middle) For each feature, we train a neural network whose goal is to reconstruct the center of the wave packet. (right) Performance of a manually engineered feature $f_E = \sum_{j=1}^N jx_j^2 / \sum_{i=1}^N x_i^2$, the first component given by Principal Component Analysis (PCA), the feature obtained at the bottleneck of an autoencoder (AE) and the one given by optimizing Renormalized Mutual Information (NN).

the encoder and an analogous network for the decoder (but we used relu activation functions in the decoders). The training parameters (optimizer, learning rate, batchsize and number of training steps) are the same as in Table I. We used $\lambda = 10^{-2}$.

Appendix G: Feature Performance in a Supervised Task

To obtain a more quantitative comparison with alternative unsupervised feature extraction techniques, we have adopted the conventional approach for comparing the performance of representations: we carry out supervised training of a neural network that takes as its input the feature. It is clear a-priori that it cannot be possible to solve arbitrary prediction tasks based on a very low-dimensional (1D or 2D) feature. However, in many physical scenarios such as the ones we consider, there are only very few underlying salient properties which might be of interest. This motivated the choice of our tasks: to predict, from the feature, the wavepacket center-of-mass or the deformation and orientation of the drop, respectively.

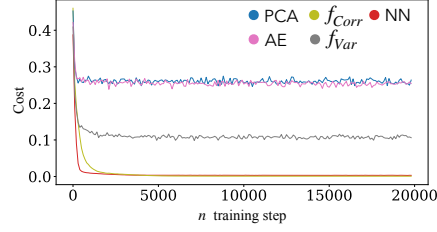
In Fig. 4a of the main text, we considered the example described in Section D 2. At fixed field fluctuation strength $\sigma_\xi = 0.38$, the supervised neural network should reconstruct the center of the wave packet, given one of the features. We use the Mean Squared Error (MSE) between the output of the network and the value of the center of the wave packet as cost function. The results are shown in Figure 6. It is evident that the feature given by optimizing Renormalized Mutual Information allows for a better performance.

In the case of the example described in Section D 3, the supervised neural network should reconstruct the orientation and deformation of the liquid drop. To reconstruct an angular variable like the orientation of the liquid drop, we cannot directly apply the mean squared error. In this case, the supervised neural network has three outputs, which will have to predict δr , $\cos 2\theta$ and $\sin 2\theta$ respectively (we remind that the boundaries of the drops look the same when rotated by π). In addition, one should take into account that the orientation of the drop can't be predicted if the deformation of the drop is close to zero. Therefore, the final cost function looks like

$$C = (n_1 - \delta r^*)^2 + \delta r^* ((n_2 - \cos 2\theta^*)^2 + (n_3 - \sin 2\theta^*)^2), \quad (\text{G1})$$

where (n_1, n_2, n_3) are the outputs of the supervised network and δr^* and θ^* the true deformation and orientation of the sample. The results are shown in Figure 7. Again we see that the feature obtained by Renormalized Mutual Information maximization allows to build a supervised network that is as accurate as that built starting from the handcrafted feature (which by design contains all the information needed to accomplish the task).

Supervised Network - Liquid Drop		
Layer	Neurons	Activation
input	2	-
layer 1	100	relu
layer 2	100	relu
output	3	linear
cost	modified MSE see Eq. G1	
optimizer	Adam	
learning rate	10^{-3}	
batch size	1500	
training steps	$2 \cdot 10^4$	



Feature	\tilde{I}	Cost
f_{Var}	1.75	0.11
f_{Corr}	3.04	0.001
PCA	1.85	0.26
AE	2.18	0.24
NN	3.21	0.003

Figure 7. Performance comparison of the supervised task in Fig. 4c of the main text. (left) Structure of the supervised neural network and optimization parameters. (middle) For each feature, we train a neural network whose goal is to reconstruct the orientation and deformation of the drop. (right) We compare the two manually engineered feature $f_{Var} = \frac{1}{N} \left(\sum_j (x_j^{(1)})^2, \sum_j (x_j^{(2)})^2 \right)$ and $f_{Corr} = \frac{1}{N} \left(\sum_j (x_j^{(1)})^2, \sum_j x_j^{(1)} x_j^{(2)} \right)$, the first component given by Principal Component Analysis (PCA), the feature given by the bottleneck of an autoencoder (AE) and that obtained by optimizing Renormalized Mutual Information (NN). We use the cost function defined in Eq. G1. The last column of the table shows the final value of the cost (Eq. G1) for each of the features.